New Efficient Substrates for Semicarbazide-Sensitive Amine Oxidase/VAP-1 Enzyme: Analysis by SARs and Computational Docking

Francesc Yraola,[†,‡] Silvia García-Vicente,[†,§] Juan Fernández-Recio,[§] Fernando Albericio,[§,||] Antonio Zorzano,[§,⊥] Luc Marti,*[,§] and Miriam Royo*[,‡]

Combinatorial Chemistry Unit and Institute for Research in Biomedicine, Barcelona Science Park, Josep Samitier 1, E-08028-Barcelona, Spain, Departament de Química Orgànica, Facultat de Química, Universitat de Barcelona, E-08028-Barcelona, Spain, and Departament de Bioquímica i Biologia Molecular, Facultat de Biologia, Universitat de Barcelona, E-08028-Barcelona, Spain

Received October 24, 2005

Structure activity relationships for semicarbazide-sensitive amine oxidase/vascular adhesion protein-1 (SSAO/VAP-1) were studied using a library of arylalkylamine substrates, with the aim of contributing to the discovery of more efficient SSAO substrates. Experimental data were contrasted with computational docking studies, thereby allowing us to examine the mechanism and substrate-binding affinity of SSAO and thus contribute to the discovery of more efficient SSAO substrates and provide a structural basis for their interactions. We also built a model of the mouse SSAO structure, which provides several structural rationales for interspecies differences in SSAO substrate selectivity and reveals new trends in SSAO substrate recognition. In this context, we identified novel efficient substrates for human SSAO that can be used as a lead for the discovery of antidiabetic agents.

Introduction

Semicarbazide-sensitive amine oxidase/vascular adhesion protein-1 (SSAO/VAP-1) is a bifunctional protein with copper-containing amine oxidase activity (EC 1.4.3.6) that converts primary amines to aldehydes, with the concomitant production of hydrogen peroxide and ammonia (Figure 1).[1,2]

SSAO/VAP-1 is highly expressed in adipocytes where it is localized mainly in plasma membrane in an insulin-independent manner.[3,4] Substrates of SSAO/VAP-1 exert a variety of insulin-like effects in human, rat, and mouse adipose cells.[4−7] Thus, substrates such as benzylamine or tyramine stimulate glucose transport in isolated human adipocytes.[7] Furthermore, in isolated rat adipocytes, the combination of substrates of SSAO with low ineffective vanadate concentrations produces a potent stimulation of glucose transport, which is abolished by semicarbazide and catalase.[4,5] This combination also induces insulin-sensitive glucose transporter isoform 4 (GLUT4) recruitment to the cell surface,[4,5] lipogenesis[8] and an inhibition of lipolysis.[7] These observations indicated that the SSAO-dependent generation of hydrogen peroxide may be responsible for these effects via a chemical interaction with vanadate, which can form peroxovanadate, a powerful insulin-mimetic agent.[9]

More recently, in vivo studies have also demonstrated the antidiabetic properties of the combination of benzylamine or other arylalkylamines with vanadium in experimental models of type 1 and type 2 diabetes.[9−11] As a beneficial effect of the administration of exogenous SSAO substrates, beyond their antidiabetic properties, we could expect a decrease in the oxidation of potential endogenous substrates, methylamine and aminoacetone, whose product of oxidation, formaldehyde, has been strongly implicated in cardiovascular pathologies associated with diabetes.[12]

On the basis of these observations, our research focuses on the identification of potent SSAO/VAP-1 substrates based on arylalkylamines. Benzylamine or arylalkylamine derivatives are good candidates, as shown by previous modeling studies of the catalytic domain of SSAO/VAP-1. We previously found that the aromatic residues Tyr 384, Phe 389, and Tyr 394 define a pocket of stable size (7 Å width), which may participate in the binding of apolar substrates.[13] After defining the pharmacophoric moiety of SSAO substrates based on benzylamine/arylalkylamine derivatives, we designed a strategy to evaluate other substrate requirements that enhance substrate-binding affinity.

Here we studied SSAO/VAP-1 structure activity relationships (SARs) and identified several molecular features using benzylamine as a hit. Our study provides key data on the differences between human and mouse SSAO substrate selectivity and contributes to the identification of new highly potent substrates. In addition, we used computational docking and homology-based modeling to analyze the results and provide a structural basis for the interaction between the arylalkylamine substrates and SSAO.

Results and Discussion

Combinatorial Chemistry. A combinatorial approach was applied to define the structural ligand requirements for new SSAO substrates. To explore the substitution of the benzylamine aromatic ring, compounds with electron-withdrawing and electron-donating groups were evaluated as ligands of the phenyl residues near the catalytic site of the enzyme. Thus, both electronic and steric effects were studied. In this context, 48 compounds were tested, combining commercial and synthesized ones (Tables 1−4 in Supporting Information). After testing the first set, we synthesized a second generation of compounds using

* Corresponding authors. Phone: +34934037122 (M.R.); +34934034700 (L.M.). Fax: +34934037126 (M.R.); +34934034717 (L.M.). E-mail: mroyo@pcb.ub.es (M.R.); lmarti@pcb.ub.es (L.M.).
[†] These authors contributed equally to the study.
[‡] Combinatorial Chemistry Unit.
[§] Institute for Research in Biomedicine.
[||] Departament de Química Orgànica.
[⊥] Departament de Bioquímica i Biologia Molecular.

10.1021/jm051076e CCC: $33.50
Published on Web 09/22/2006

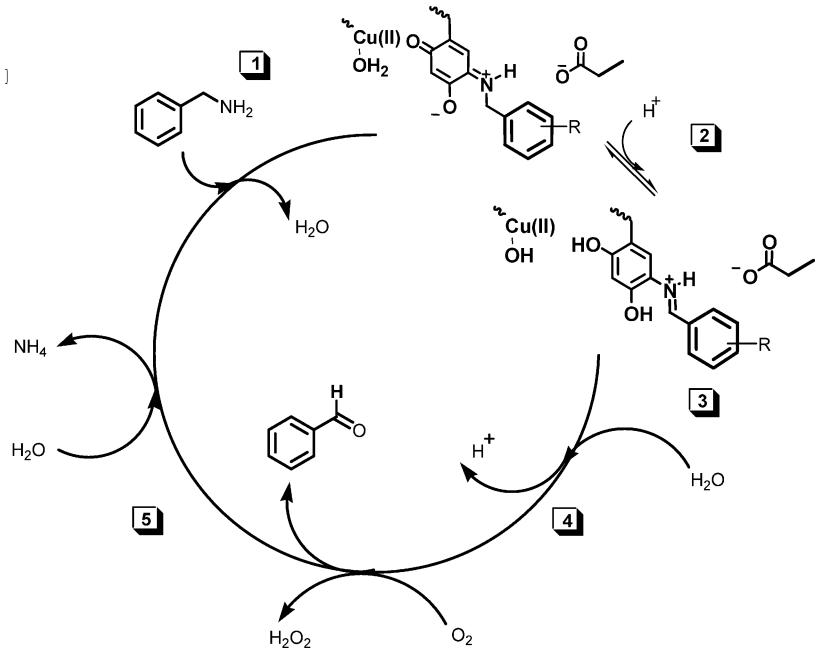

Figure 1. SSAO turnover is schematically represented. (1) Benzylamine condensation to topaquinone cofactor of the enzyme (TPQ); (2) tautemerization of Schiff base intermediate (rate-limiting step); (3), (4), and (5) hydrolysis followed H_2O_2 and ammonia production and aldehyde byproduct release.

compound **12** as a starting point. This second generation, based on the modification of the amino group of *m*-xylylenediamine, was also synthesized by a solid-phase approach (Table 3 in Supporting Information). The members of this new family were designed and synthesized, exploring size, hydrophobicity, and stability by new hydrogen-binding interactions in this extended position. The function of this extended group was to fill the extra apolar cavity (defined by Leu 469 and Phe 389 residues), found in previous studies, to enhance binding capacity to the SSAO active site.[13,17] After screening, the compounds that showed substrate properties were selected, resynthesized, and purified to confirm the biological data and establish SARs. The selected compounds were classified in two structural families: (a) arylalkylamines, especially with *para* substitution on the aromatic ring, and (b) *m*-xylene derivatives.

Synthesis of Selected Compounds. The arylalkylamines selected were prepared from commercially available aldehydes by reductive amination. First, the hydroxylamine was condensed with aldehyde in methanol at reflux for 30 min. In all the cases, the reaction quantitatively yielded the corresponding aldoximes. The aldoxime was then catalytically reduced with $PtO_2 \cdot 1H_2O$ and H_2 (4 bar) in acetic acid at room temperature. The conversion is directly proportioned to the nature of the substitution. In this regard, the conversions of (4-ethylphenyl)methylamine (**5**) and (3-fluoro-4-methylphenyl)methylamine (**16**) were 60 and 53%, respectively. In contrast, the conversion of (4-butylphenyl)methylamine (**11**) was 80%. In the case of strong *p*-EWG in the aryl moiety, such as (4-fluorophenyl)methylamine (**3**) and (4-(trifluoromethyl)phenyl)methylamine (**8**), the reduction by $PtO_2 \cdot 1H_2O$ was not successful. Other catalysts were tested, such as Pd/C or $Pd(OH)_2$, with similar unsuccessful results. This could be explained by strong electropositive density of the carbon between the Ph rings of the corresponding aldoximes. In these cases, the reduction was carried out using hydride reagent $LiBH_4$ under Ar refluxed in dry THF. Under these conditions, compounds **3** and **8** were obtained with a moderated yield but with good purity (over 99% in both cases). The corresponding hydrochloride salts were obtained by treatment with HCl in dioxane using ethyl acetate or diethyl ether as precipitating solvents (Scheme 1).[14]

Scheme 1[a]

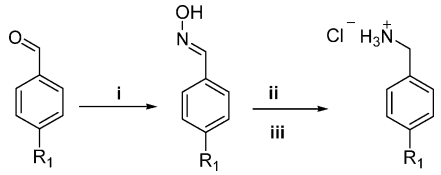

[a] Reagents and conditions: (i) NH_2OH, 2 h at room temperature; (ii) H_2 (4 bar)/ $PtO_2 \cdot 1H_2O$, 24 h at room temperature or $LiBH_4$ in THF for 8 h; (iii) HCl/dioxane.

A second generation of compounds derived from compound **12** were synthesized using the commercial 3-(Boc-aminomethyl)-benzylamine hydrochloride as starting material. Next, several standard protocols were applied to obtain the desired compounds in the reactions represented in Scheme 2. To obtain compound **12**, 3-(Boc-aminomethyl)-benzylamine hydrochloride was acylated quantitatively with acetic anhydride and base. In the case of *N*-(3-aminomethyl-benzyl)-acylamide derivatives (compounds **31**, **32**, **34**, **38**, **39**, and **40**), 3-(Boc-aminomethyl)-benzylamine hydrochloride was acylated with the corresponding carboxylic acids and as coupling mixture reagents HOBt, DIPCDI, and DIEA. The Boc-protected compounds were yielded after purification. The allylcarbamate derivative **33** was obtained by reaction of 3-(Boc-aminomethyl)-benzylamine hydrochloride with allyl chloroformate, giving quantitative yields of the corresponding Boc-protected compound **33**. Compound **35** was obtained first by acylating 3-(Boc-aminomethyl)-benzylamine with FmocPhg and as coupling reagents HOBt and DIPCDI. The Fmoc protecting group was then removed, and the final compound was achieved by acylation with acetic anhydride. The sulfonamide derivative **36** was achieved by reacting 3-(Boc-aminomethyl)-benzylamine hydrochloride with tosyl chloride, yielding the Boc-protected derivative **36**.[15] The hydrochloric salts were obtained quantitatively by treatment with HCl in dioxane of the Boc derivatives using ethyl acetate or diethyl ether as solvent.

Scheme 2[a]

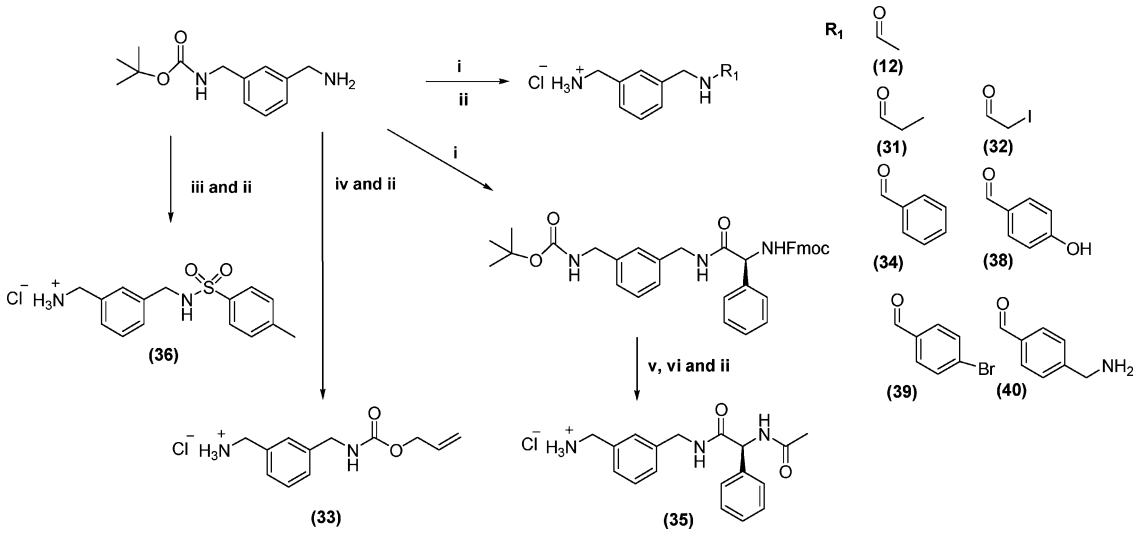

[a] Reagents and conditions: (i) 3-(Boc-aminomethyl)-benzylamine hydrochoride/RCOOH/HOBt/DIPCDI/DIEA in DMF, 12 h at room temperature; (ii) HCl/dioxane, 2 h at room temperature; (iii) $ClSO_2p$-Ts/K_2CO_3 in acetone/water, 4 h at room temperature; (iv) allyl chloroformate/DIEA in DCM for 4 h at room temperature; (v) piperidine/DMF, 4 h at room temperature; (vi) Ac_2O/DIEA in DCM, 4 h at room temperature.

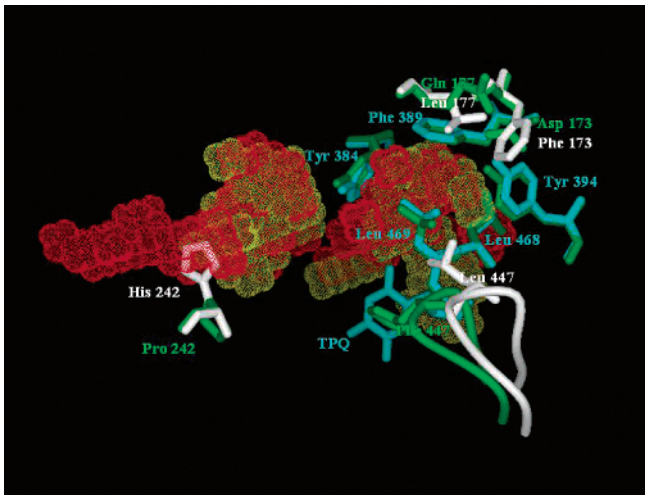

Figure 2. Comparison of mouse and human SSAO active sites. Active site residues in human SSAO are shown in cyan. Residues near the human SSAO active site that are nonconserved in mouse SSAO are in white. The equivalent residues in mouse SSAO are in green. Binding cavities are shown as dots (human in yellow; mouse in red), which were computed with Pocket-Finder (www.bioinformatics.leeds.ac.uk/pocketfinder/). Figure prepared with ICM-Browser from Molsoft (www.molsoft.com).

Table 1. Human and Mouse SSAO Activity in the Presence of Arylalkylamine Derivatives Synthesized as SSAO Substrates[a]

		SSAO activity (% rel. to benzylamine oxidation)	
entry	compound	human	mouse
1	benzylamine	100 ± 7	100 ± 15
3	4-fluorobenzylamine	134 ± 11	127 ± 4
5	4-ethylbenzylamine	14 ± 1	26 ± 3
8	4-trifluoromethyl-benzylamine	4 ± 1	35 ± 3
11	4-butylbenzylamine	5 ± 1	24 ± 3
16	3-fluoro-4-methyl-benzylamine	88 ± 2	133 ± 2
41	phenylethylamine	21 ± 2	19 ± 2
42	3-phenylpropylamine	44 ± 4	40 ± 5
44	4-phenylbutylamine	166 ± 11	71 ± 4
46	2-(4-fluorophenyl)-ethylamine	35 ± 3	18 ± 2

[a] Human and mouse SSAO activity was determined by detecting the production of hydrogen peroxide in the presence of distinct compounds present at 1 mM for human and 100 μM for mouse activity measurements, as indicated in Materials and Methods. Values are means of percentages relative to benzylamine-related hydrogen production.

Exploration of Human and Mouse Substrate Selectivity by Docking. Slight changes of the substituents on the phenyl group of benzylamines produced a considerable decrease in the catalytic activity of the two enzymes. As expected, more substrates for mouse than for human SSAO were found (Tables 1−4 in Supporting Information). These results are in agreement with previous observations that human SSAO/VAP-1 is more restrictive in substrate selectivity than the mouse enzyme.[16] This observation could be attributed to differences in the distribution of the mouse and human catalytic site residues. As previously proposed by Wilce et al., amine oxidase substrate recognition may be influenced by the amino acid composition of the channel near the junction of domains D3 and D4 of the protein, which form the entrance of the substrate from the protein surface to the active site.[17] Because of their critical position within the catalytic site, Tyr 384 or Leu 468 and Leu 469 residues may affect the substrate selectivity of the enzyme.[9,17−19] However, because these same residues are conserved in mouse SSAO/VAP-1, their nature cannot explain the difference in substrate selectivity observed between the two species. To perform a more detailed comparison of mouse and human SSAO active sites at the structural level, a model of mouse SSAO was built based on the structure of the homologous human SSAO protein (PDB code 1us1). Superimposition of mouse and human SSAO active sites showed that the conformation of the catalytic residues is well-conserved, as expected (Figure 2). However, the active site in mouse SSAO model was slightly larger than that in human SSAO X-ray structure. To evaluate whether this was artifactual (because we were comparing a homology-based model and an X-ray structure) and also to check the dynamic behavior of the active site, we performed molecular dynamics simulations on both structures, as described in the Experimental Section. We extracted snapshots from the simulations every 10 ps and computed the solvent-excluded volume of the active site in these conformations using Pocket, a program that identifies active sites of proteins on the basis of the Alpha Shape theory.[20] A few outlier conformations for which Pocket artificially detected the active site as "fused" with other larger cavities, or

Table 2. Human and Mouse SSAO Activity in the Presence of Arylalkylamine Derivatives Synthesized as SSAO Substrates[a]

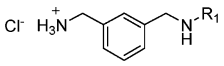

(II)

entry	compound	SSAO activity (% relative to benzylamine oxidation)	
		human	mouse
12		3 ± 1	16 ± 4
31		4 ± 1	27 ± 1
32		38 ±3	61 ± 5
33		21 ± 1	49 ± 3
34		17 ±1	58 ± 4
35	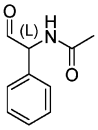	2 ±1	13 ± 3
36	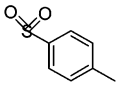	12 ±2	14 ± 3
38	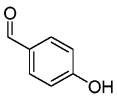	5 ±1	26 ± 1
39	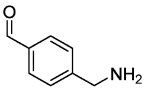	17 ± 2	12 ± 1
40	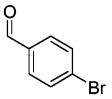	16 ± 2	46 ± 1

[a] Human and mouse SSAO activity was determined by detecting the production of hydrogen peroxide in the presence of distinct compounds present at 1 mM for human and 100 μM for mouse activity measurements, as indicated in Materials and Methods. Values are means of percentages relative to benzylamine-related hydrogen production.

"fragmented" in small cavities, were not considered for calculations. The average volumes of the SSAO active sites during simulations were similar in mouse ($V = 190.6$ Å^3 ± 13.4 SD) and in human ($V = 185.0$ Å^3 ± 37.9 SD). However, the larger deviation in volume values for human SSAO indicate that its active site is more flexible than that of mouse. There were also interesting differences in the residues near the active site. For instance, Phe 173 at the entrance of the active site in human SSAO is Asp 173 in mouse, which leaves more space at the entrance of the active site and introduces an attraction point for positively charged substrates. Another residue, Leu 177 in human SSAO, is Gln 177 in mouse, whose side-chain conformation makes the entrance of the active site wider. All the considerations described above might explain the differences in substrate affinity between human and mouse SSAO. Another potentially interesting difference is that human His 242 is mutated to Pro 242 in mouse, which creates a small cavity adjacent to the catalytic site. Interestingly, this proline residue is also conserved in bovine SSAO (Pro 241). The role of this cavity is unknown. Some insights will be provided by docking simulations, as discussed at the end of the section. Finally, in the amine oxidase family of enzymes, intersubunit interactions are formed by two long hairpins. One of these, the β-ribbon arm I, which stretches along the surface of the molecule to the channel entrance, may also be involved in substrate specificity because the residues at the end of the arm differ in each protein.[17] For instance, Leu 447 in this loop in human SSAO is Phe 447 in mouse. This loop differs between human and bovine SSAO in only two residues (Leu 447, Tyr 448 in human vs Phe 446, Leu 447 in bovine). Despite this small difference in

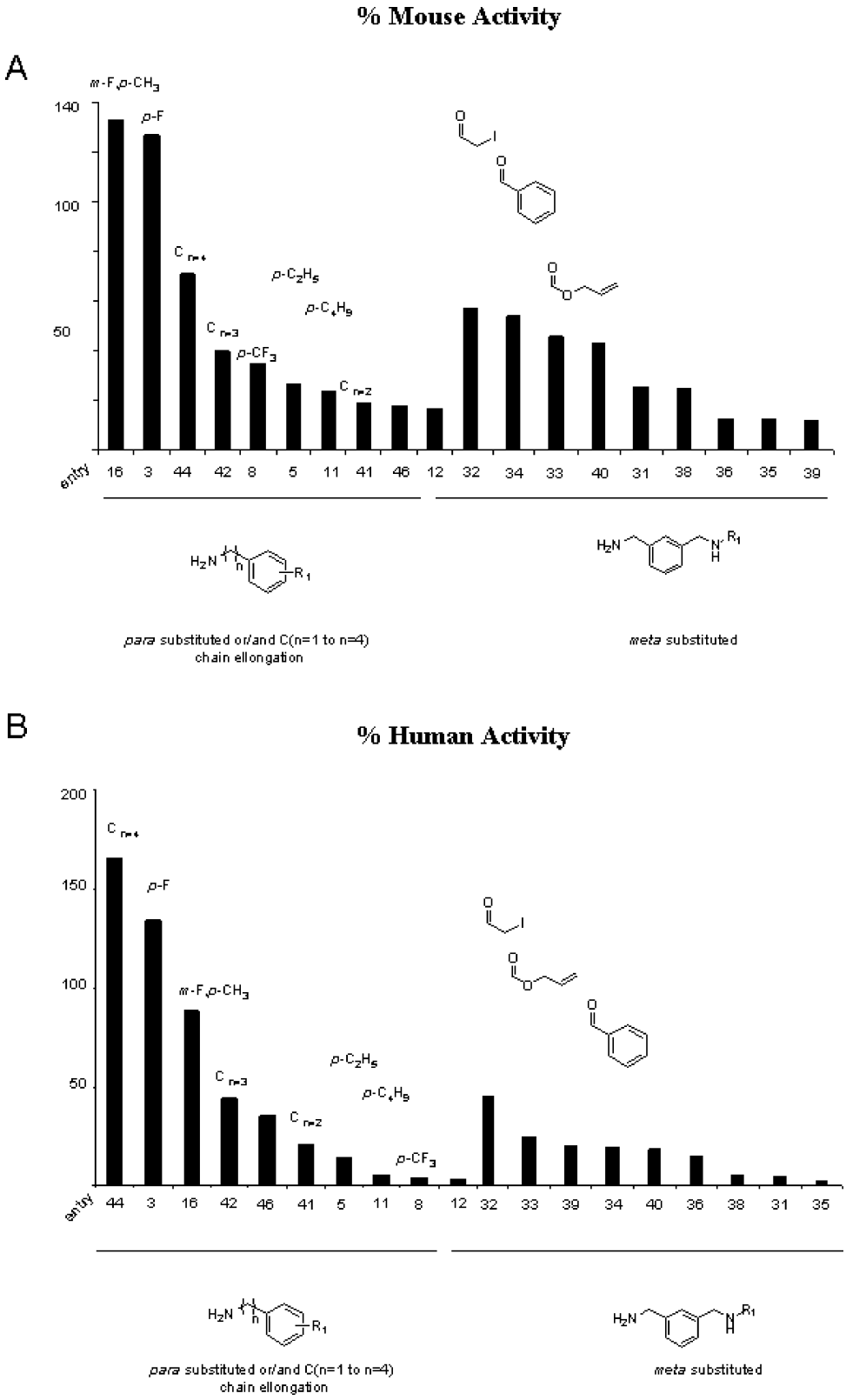

Figure 3. Qualitative representation of % mouse (A) and human SSAO activity (B). Values extracted from Tables 1 and 2.

sequence, the overall loop conformation is distorted. In our model of mouse SSAO, the loop conformation was inherited mostly from the human structure; nevertheless, there was significant conformational change with respect to the human template (Figure 2). Conformational variability of this loop during molecular dynamics was very similar in human and in mouse SSAO, ranging from 0.2 to 1.3 Å RMSD in human and from 0.2 to 1.5 Å RMSD in mouse (only Cα atoms considered). However, given the sensitivity of this loop to the residue sequence, we cannot rule out that further conformational deviation in mouse with respect to human SSAO affects the active site entrance. To our knowledge, this is the first study to provide a rational explanation of the basis of structural differences to support the interspecies differences in substrate selectivity observed between mouse and human SSAO.

Table 3. Kinetic Parameters for Mouse SSAO/VAP-1 Substrates[a]

entry	compound	K_m (μM)	V_{max} (nmol/min/mg protein)	k_{cat}[a] (s^{-1})	k_{cat}/K_m (s^{-1} M^{-1})
1	benzylamine	15.4 ± 2.2	3.5 ± 0.4	0.18	11 763
3	4-fluorobenzylamine	15.7 ± 0.4	4.4 ± 0.7	0.23	14 553
16	3-fluoro- 4-methylbenzylamine	14.8 ± 1.7	4.0 ± 0.6	0.21	14 064
32	*N*-(3-(aminomethyl)benzyl)-2-iodoacetamide	29.8 ± 3.9	2.5 ± 0.3	0.13	4428
33	*N*-allyl 3-(aminomethyl)benzylcarbamate	11.5 ± 1.2	1.8 ± 0.2	0.09	8099
34	*N*-(3-(aminomethyl)benzyl)benzamide	12.8 ± 1.6	2.1 ± 0.2	0.11	8747
41	phenylethylamine	34.8 ± 8.2	1.2 ± 0.1	0.06	1773
42	3-phenylpropylamine	27.0 ± 5.1	2.6 ± 0.5	0.13	4957
44	4-phenylbutylamine	11.3 ± 0.8	3.6± 0.2	0.19	16 664
46	2-(4-fluorophenyl)-ethylamine	88.8 ± 0.8	1.5 ± 0.2	0.08	883

[a] Kinetic parameters of human SSAO activity in the presence of the substrates indicated were determined as explained in Materials and Methods. Values are the means of four independent measurements.

Table 4. Kinetic Parameters and Docking Energy Values for Human SSAO/VAP-1 Substrates[a]

entry	compound	K_m (μM)	V_{max} (nmol/min/mg protein)	k_{cat} (s^{-1})	k_{cat}/K_m (s^{-1} M^{-1})	docking energy (kcal/mol)
1	benzylamine	224 ± 54	315 ± 17	0.45	2023	−68.8
3	4-fluorobenzylamine	205 ± 18	490 ± 45	0.71	3439	−67.6
16	3-fluoro-4-methylbenzylamine	405 ± 34	398 ± 44	0.57	1413	−65.3
32	*N*-(3-(aminomethyl)benzyl)-2-iodoacetamide	525 ± 36	263 ± 17	0.38	720	−46.4
33	*N*-allyl 3-(aminomethyl)-benzylcarbamate	569 ± 32	114 ± 9	0.16	289	−30.5
34	*N*-(3-(aminomethyl)benzyl)benzamide	630 ± 55	112 ± 5	0.16	256	−26.6
41	phenylethylamine	3725 ± 1007	288 ± 39	0.41	111	−72.7
42	3-phenylpropylamine	1672 ± 192	342 ± 42	0.49	294	−63.8
44	4-phenylbutylamine	280 ± 40	571 ± 20	0.82	2938	−69.1
46	2-(4-fluorophenyl)ethylamine	1895 ± 347	300 ± 40	0.43	228	−72.2

[a] Kinetic parameters of mouse SSAO activity in the presence of the substrates indicated were determined as described in Materials and Methods. Values are means of four independent measurements.

Qualitative Structure Activity Relationships. All resynthesized compounds were screened again as potential substrates of mouse and human SSAO. As described above, these selected compounds can be classified in two structural families: (a) phenylalkylamines (Table 1) and (b) derivatives of *m*-xilene diamines (Table 2).

The phenylalkylamine active compounds present diverse substitutions in the aryl ring, especially in the *para* position, which appears to be crucial for the SSAO activity (Table 1). The percentage of mouse SSAO activity of the *p*-substituted benzyl compounds decreased with the presence of bulky *para*-substitution groups (Figure 3A). A similar effect was observed for human SSAO (Figure 3B), where compound *p*-F (**3**) showed remarkably higher activity than benzylamine (**1**).

To minimize the possible substitution aryl ring effects in the interaction with the SSAO active site, distinct compounds with diverse C chain lengths between the amino group and the phenyl group were explored. With this purpose, commercial arylalkylamines were tested (Table 1, compounds **41**, **42**, and **44**), among these, phenylethylamine, and already known SSAO substrate.[27] For these compounds, mouse SSAO activity increased as the chain length between the amine function and the phenyl ring was enlarged. In this regard, these compounds showed the following decreasing relation: C $n = 4$ (**44**) > C $n = 3$ (**42**) > C $n = 2$ (**41**) (Figure 3A). When these compounds were tested with human SSAO (Figure 3B), similar effects were observed and compound C $n = 4$ (**44**) showed higher activity than benzylamine (**1**).

The biological activity of compounds with modified amino group of *m*-xylylenediamine (Table 2) showed that the increase in volume was well-tolerated by the catalytic site of mouse SSAO (Figure 3A). For the human enzyme, the addition of hydrophobic groups also induced the recovery of significant activity (compounds **32**−**34**, **39**, and **40**). The affinity preferences of the hydrophobic group are consistent with the previous structural studies of the active site, which defined an extra cavity of highly hydrophobic character.[13,17]

QSAR Based on Kinetic Studies. The kinetic parameters for the selected novel mouse and human SSAO substrates were determined (Tables 3 and 4). The k_{cat} of human and mouse VAP-1 for benzylamine was relatively low (0.18 and 0.45 s^{-1}, respectively). As previously reported, this low catalytic turnover may support the implication of VAP-1/SSAO in lymphocyte adhesion.[21] High affinity substrates for mouse and human SSAO were found.

Interestingly, compound **44**, with a chain length of four C, showed a 2-fold V_{max} and, similar to fluorinated benzylamine compounds **3** and **16**, a better catalytic efficiency (k_{cat}/K_m) than benzylamine in both species. In the case of 4-phenybutylamine (**44**), the aromatic ring may be at a sufficient distance to prevent π-stacking interactions between the phenyl ring of the arylalkylamine and the SSAO active site.

We observed a significant trend between the k_{cat} for the mouse and human SSAO (Figure 4). A first interpretation of this observation is that, beyond differences in substrate selectivity, mouse and human SSAO have a similar capacity to catalyze amines. Up to certain point, a good substrate for mouse SSAO has high probability of also being a good substrate for human SSAO. Similarly, a bad substrate for mouse SSAO will probably be a bad substrate for the human enzyme as well (Figure 4). This is relevant for the design of future screenings. However, as shown by the intercept of the fitted line, a bad substrate for mouse SSAO may not be a substrate for human SSAO[22] (Tables 1−2).[22] It is interesting to note that (1) SSAO activity is sensitive to *meta* substitutions, (2) compounds **41** and **46** phenylethylamine compounds are equally poor substrates for mouse and human SSAO, and (3) the presence of a fluor atom in the *para* position and the length of the aliphatic chain greatly influence

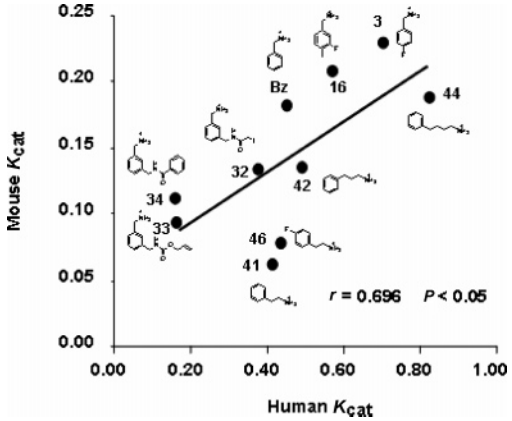

Figure 4. Correlation of mouse SSAO/VAP-1 k_{cat} versus human k_{cat} SSAO/VAP-1 values extracted from Tables 3 and 4, respectively.

the capacity of the compound to be oxidized by both human and mouse SSAO. Among the compounds, we identified **3**, **16**, and **44** as the best substrates in both species.

Qualitative SARs and Docking. To provide a structural basis to our observations, we performed computational docking studies using the X-ray structure of human SSAO, which is available in the PDB with code 1us1. Compounds **1**, **3**, **16**, **32**−**34**, **41**, **42**, **44**, and **46** were computationally docked onto the coordinates of human SSAO. Given that Leu469 partially occluded the active site, we modeled a distinct rotamer of the leucine side-chain, which resulted in a slightly more open active site. The conformation of TPQ in the human structure (1us1) was incompatible with catalysis. Therefore, it was modeled to the active conformation (so-called "off-Cu") using the coordinates of SSAO from *Escherichia coli* of code 1spu as template.[23] The overall docking results did not depend heavily on the TPQ conformation, but the ammonium group of the ligand compounds was consistently closer to the TPQ moiety when the latter was in the "off-Cu" conformation. Figure 5 shows the lowest-energy docking conformations obtained for selected compounds. As expected, the docking orientation obtained for benzylamine (**1**) fitted the active site perfectly (Figure 5A), with the ammonium group close to the catalytic oxygen atom of TPQ. Regarding the docking results of 4-phenylbutylamine (**44**), the lowest-energy docking conformation superimposed nicely onto the benzylamine (**1**) docking structure (Figure 5B). The ammonium group of **44** was located in the same spatial coordinates as that in benzylamine, and the four Caliphatic chain superimposed perfectly onto the aromatic ring of benzylamine. Thus, the aromatic ring of **44** was closer to the active site entrance, without major atomic clashes with surrounding protein atoms. As expected, this interaction mode proposed by the docking calculations indicates that the aliphatic chain has favorable interactions with the active site, while the phenyl ring prevents excessive π-stacking with this site, perhaps favoring the exit of the aldehyde byproduct. Several of the docking orientations of benzylamine (**1**) were found in the adjacent cavity around His 242; this was not observed for **44**. We can hypothesize that bulkier compounds such as **44** are not trapped inside the human SSAO active site as easily as benzylamine (**1**), which would explain why the V_{max} of **44** is larger than that of **1** (Table 4). In contrast, the larger active site (including the mouth entrance and this adjacent cavity of unknown role) in mouse SSAO (Figure 2) might equally trap small-sized and bulkier compounds (Table 3). This hypothesis is therefore consistent with the experimental data. Compounds **3**, **16**, **41**, **42**, and **46** had similarly good docking energy values (Table 4), and their

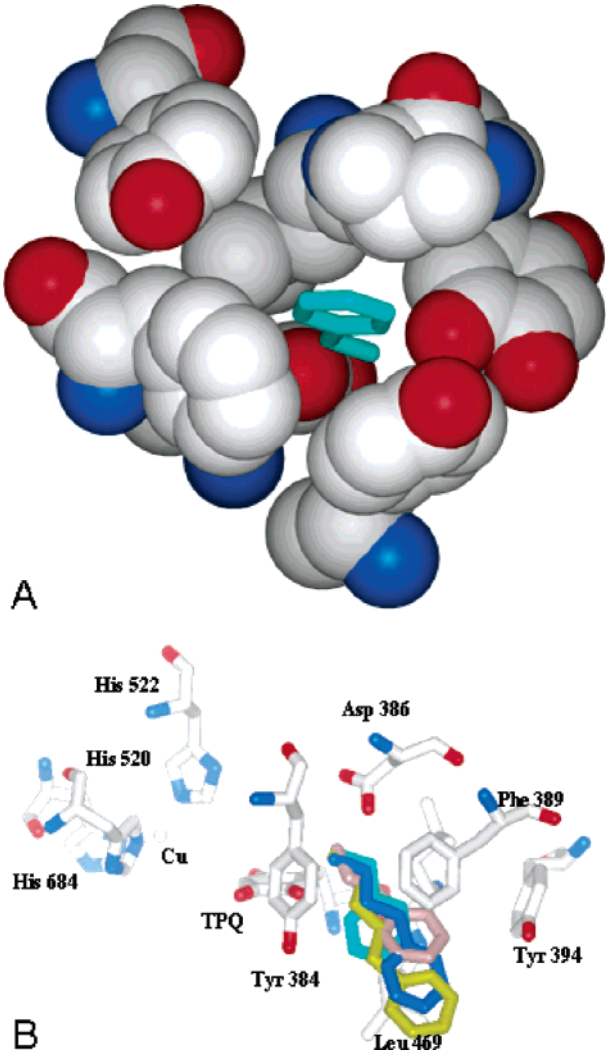

Figure 5. Computational docking results. (A) Best docking solution (lowest binding energy) calculated by CMIP for compound **1** (stick representation, color cyan), surrounded by human SSAO active site residues (represented in CPK). (B). Best docking solutions for compounds **1** (cyan), **41** (pink), **42** (blue), and **44** (yellow) on the active site of human SSAO. Figure prepared with ICM-Browser from Molsoft (www.molsoft.com).

lowest-energy docking solutions were found within the active site in a similar orientation as in **1** and **44**. Interestingly, the docking structure of phenylethylamine (**41**) deviated slightly from compounds **1** and **44**, indicating that it does not fit as perfectly into the active site. This observation is consistent with the lower affinity found for **41** and for its fluoroderivative (compound **46**). Regarding **42**, the atoms of the phenyl ring were located between the corresponding atoms of compounds **41** and **44**, but slightly closer to the latter. The distance between the center of atomic coordinates of the phenyl ring in compounds **41** and **44** is 3.21 Å, whereas the equivalent distance between **42** and **41** is 2.03 Å, and the one between **42** and **44** is 1.21 Å. This may explain why the activity found experimentally is below that of benzylamine (**1**). In contrast, compounds **33** and **34**, which showed poor experimental k_{cat} values with human SSAO, did not yield any docking orientation within the active site where the ammonium group can be at a reasonable distance from TPQ. In addition, the binding energy of **33** and **34** docking solutions, located at the entrance of the active site but not within it, were much worse than those of the "good" substrates. Interestingly, compound **32**, which has an intermediate experimental K_{cat}

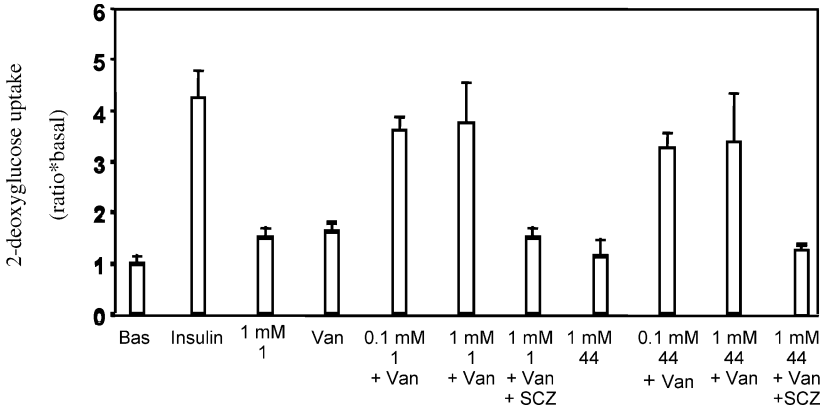

Figure 6. Stimulation of glucose transport in isolated mouse adipocytes. Mouse adipocytes were incubated for 45 min without (bas) or with 100 nM insulin, amines at the indicated concentration (**1**, benzylamine, **44**, 4-phenyl-butylamine) alone or in combination with 1 mM sodium orthovanadate (Van) and/or 1 mM semicarbazide (SCZ), as indicated. Subsequently, 2-deoxy-D-glucose uptake was measured over a 10-min period. Results are mean ± SEM of two experiments performed in triplicate.

value, had a few docking orientations within the active site, with a binding energy between that of the good substrates and the poor ones. This observation correlates with the experimental k_{cat} values of these compounds. This is remarkable considering that enzymatic activity can be affected by determinants other than binding affinity of the substrates, and that our model is limited by the use of a rigid-body approach for the active-site side-chains. In fact, compounds **1**, **41**, and **46** had slightly larger computed binding energy values than the ones expected from the energy/k_{cat} relation for the similar compounds **3**, **42**, and **44**. Indeed, the side-chain of Leu469 was very close to the aromatic ring of these compounds, so the conformation of this residue might affect compounds **1**, **41**, and **46** in a different way than to the others. Although this is out of the scope of this work, we are planning a systematic study in which protein flexibility will be analyzed.

Activation of Glucose Transport in Isolated Mouse Adipocytes. The incubation of isolated rat or mouse adipocytes in the presence of SSAO substrates, such as benzylamine and vanadate, stimulates glucose transport.[4,5] Here we analyzed whether one of our best novel SSAO substrates (**44**) exerted such an insulin-mimetic effect. The incubation of isolated mouse adipocytes with 0.1 or 1 mM of compound **44** plus vanadate produced a strong stimulation of glucose transport (3.3-fold and 3.4-fold, respectively), similar to that obtained with insulin or benzylamine plus vanadate (Figure 6). As for benzylamine, this effect was completely inhibited by semicarbazide. The incubation of 1 mM of compound **44** without vanadate did not significantly affect glucose transport (1.1-fold).

Conclusions

Here we derived SARs for SSAO /VAP-1 with 20 aryalkylamine analogues selected from a library of 48 compounds. The chemical nature of the substitution in the aromatic ring and the length of the alkyl chain modulates their activity versus SSAO/VAP-1. This finding introduces a new concept in SSAO substrate design that could be useful in subsequent studies.

More importantly, three novel SSAO substrates, namely, 4-fluorobenzylamine (**3**), 3-fluoro-4-methyl-benzylamine (**16**), and 4-phenylbutylamine (**44**), were identified. These compounds presented high affinity for mouse and human SSAO, and their V_{max} values were even higher for the latter. Results from docking calculations were consistent with these experimental values. Lowest-energy binding modes fitted nicely within the active site and had the ammonium group near the TPQ residue.

Compound **44** is, to our knowledge, the best substrate described to date for human SSAO. Interestingly, this compound is structurally related to the side chain of lysine, an endogenous amino acid that interacts with the human catalytic site of SSAO/VAP-1.[32] We also show that compound **44** strongly stimulated glucose transport in isolated mouse adipocytes.

Experimental Section

Materials and Methods. DIPCDI was obtained from Fluka Chemika (Buchs, Switzerland) and HOBt from Albatross Chem, Inc. (Montreal, Canada). 3-(Boc-aminomethyl)-benzylamine hydrochoride was purchased from Neosystem (Strasbourg, France). Semicarbazide hydrochloride, benzylamine hydrochloride, hydrogen peroxide, sodium orthovanadate horseradish peroxidase, and other chemicals were purchased from Sigma Aldrich (St. Louis, MO, U.S.A.). Purified human VAP-1 was a kind gift from BioTie Therapeutics (Turku, Finland). Amplex red reagent (10-acetyl-3,7-dihydroxyphenoxazine) was from Molecular Probes (Eugene, OR, U.S.A.). 2-Deoxy-D-[2,6-3*H*]glucose (53 Ci/mmol) was purchased from Amersham Pharmacia Biotech (Buckinghamshire, U.K.). Purified porcine insulin was a kind gift from Eli Lilly (Indianapolis, IN). Collagenase type I was obtained from Worthington (Lakewood, NJ). Other chemicals were obtained from Aldrich (Milwaukee, WI., U.S.A.), with the highest purity grade available. All commercial reagents and solvents were used as received. The $^{1}H/^{13}C$ NMR spectra were recorded on a Varian Mercury 400-MHz spectrometer. HPLC analysis was performed using an Alliance 2795 Waters Chromatography system with a reverse-phase column C_{18} X-Terra 3.5 μm 2.1 × 50 mm column with Waters 996 PDA detector. HPLC-MS spectra were recorded on a Waters Alliance HT 2795 system with dual λ absorbance detector 2487 and Micromass ZQ mass spectrometer. The purity of the arylalkylamines synthesized was determined by HPLC using two gradients, see Supporting Information for HPLC purity data table and spectroscopy data ($^{1}H/^{13}C$ NMR) of selected compounds resynthesized.

Synthesis of Aldoxime Derivatives. The corresponding aldehyde (300 mg) was dissolved in methanol (5 mL). After that, a solution of hydroxylamine in water at 50% (4 mmol) was added, and the mixture was refluxed for a period of 30 min. The solvent was then evaporated, and the resulting solid was dissolved in ethyl acetate (100 mL) and washed with HCl 1 N (2 × 100 mL), saturated $NaHCO_3$ (2 × 100 mL) solution, and brine (2 × 100 mL). The organic phase was dried with $MgSO_4$ and concentrated at reduced pressure to give the corresponding aldoxime. The compounds were analyzed by HPLC-MS.

Synthesis of the Arylalkylamine Derivatives. Method A. The corresponding aldoxime (300 mg) and $PtO_2 \cdot 1H_2O$ (0.022 mmol) were dissolved in acetic acid (10 mL). The mixture was pressurized with H_2 to 4 bar and reacted for 8 h at room temperature. The

crude was then filtered through Celite, the acetic acid was removed at low pressure, and the crude product was dissolved with HCl 1 N (300 mL). The aqueous phase was washed with ethyl acetate (3 × 100 mL), and the organic layer was discarded. The aqueous phase was then basified with a solution of NaOH 1 M and washed with ethyl acetate (3 × 100 mL). The organic phase was dried with $MgSO_4$ and concentrated at reduced pressure to give the corresponding amine. Afterward all the compounds were treated with 2 mL of HCl/dioxane 4.0 M in 10 mL of ethyl acetate for 2 h at room temperature. The final hydrochloride salts were filtered and dried.

Method B. The corresponding aldoxime (300 mg) was dissolved with 5 mL of $LiBH_4$ 4.0 M in dry THF and refluxed for 8 h. Then 100 mL of ethyl acetate and 100 mL of HCl 6 N were added to the crude product. The aqueous phase was washed with ethyl acetate (3 × 100 mL), and the organic layer was discarded. The aqueous phase was then basified with a solution of NaOH 1 M and was washed with ethyl acetate (3 × 100 mL). The organic phase was dried with $MgSO_4$ and concentrated at reduced pressure to give the corresponding amine. Afterward, all the compounds were treated with 2 mL of HCl/dioxane 4.0 M in 10 mL of ethyl acetate for 2 h at room temperature. The final hydrochloride salts were filtered and dried.

(4-Fluorophenyl)methylamine Hydrochloride Salt (3). A white solid with 99% purity was obtained following method B (yield = 40%). ^{1}H NMR (CD_3OD, 400 MHz): 4.06 (s, 2H), 7.06 (dd, 2H, J = 6.1 Hz, J = 11.4 Hz), 7.31 (dd, 2H, J = 5.4 Hz, J = 8.2 Hz). ^{13}C NMR (CD_3OD, 400 MHz): 40.7, 115.5, 130.4, 132.7, 161.0, 163.4. ES+ (m/z): calcd for $C_7H_9F_1N_1$ $(M + H)^+$, 126.0714; found, 126.0715.

(4-Ethylphenyl)methylamine Hydrochloride Salt (5). A white solid with 100% purity was obtained following method A (yield = 60%). Compound **5** was recrystallized with *i*-PrOH/MeOH (2:1) at 75 °C. ^{1}H NMR (CD_3OD, 400 MHz): 1.22 (t, 3H, J = 7.6 Hz), 2.66 (q, 2H, J = 7.6 Hz), 7.28 (d, 2H, J = 8.1 Hz), 7.36 (d, 2H, J = 8.1 Hz). ^{13}C NMR (CD_3OD, 400 MHz): 14.8, 28.3, 42.9, 128.4, 128.8, 130.4, 145.6. ES+ (m/z): calcd for $C_9H_{14}N$ $(M + H)^+$, 136.1121; found, 136.1123.

(4-(Trifluoromethyl)phenyl)methaylamine Hydrochloride Salt (8). A white solid with 95% purity was obtained following method B (yield = 45%). ^{1}H NMR (CD_3OD, 400 MHz): 4.22 (s, 2H), 7.76 (d, 2H, J = 8.1 Hz), 7.67 (d, 2H, J = 8.2 Hz). ^{13}C NMR (CD_3OD, 400 MHz): 42.5, 125.7, 125.8, 125.8, 125.9, 129.5, 137.6. ES+ (m/z): calcd for $C_8H_9F_3N$ $(M + H)^+$, 176.0682; found, 176.0680.

(4-Butylphenyl)methylamine Hydrochloride Salt (11). A white solid with 100% purity was obtained following method A (yield = 79%). ^{1}H NMR (CD_3OD, 400 MHz): 0.93 (t, 3H, J = 7.4 Hz), 1.35 (m, 2H), 1.59 (m, 2H), 2.64 (t, 2H, J = 7.7 Hz), 4.06 (z, 2H), 7.26 (d, 2H, J = 7.9 Hz), 7.36 (d, 2H, J = 8.0 Hz). ^{13}C NMR (CD_3OD, 400 MHz): 13.0, 22.0, 33.6, 35.0, 42.9, 128.7, 129.0, 130.4, 144.1. ES+ (m/z): calcd for $C_{11}H_{18}N$ $(M + H)^+$, 164.1434; found, 164.1433.

(3-Fluoro-4-methylphenyl)methylamine Hydrochloride Salt (16). A white solid with 98% purity was obtained following method A (yield = 53%). Compound **16** was recrystallized with *i*-PrOH/MetOH (85:5) at 75 °C. ^{1}H NMR (CD_3OD, 400 MHz): 2.28 (s, 3H), 4.06 (s, 2H), 7.09 (t, 1H, J = 9.0 Hz), 7.30 (ddd, 1H, J = 2.3 Hz, J = 4.7 Hz, J = 7.3 Hz), 7.35 (d, 1H, J = 7.2 Hz). ^{13}C NMR (CD_3OD, 400 MHz): 13.1, 13.2, 42.4, 115.2, 128.3, 132.4, 160.5, 163.0. ES+ (m/z): calcd for $C_7H_9F_1N_1$ $(M + H)^+$, 140.0870; found, 140.0871.

***N*-(3-(Aminomethyl)benzyl)acetamida Hydrochloride Salt (12).** 3-(Boc-aminomethyl)-benzylamine hydrochloride (300 mg, 1 equiv) was acetylated with Ac_2O/DIEA (1:2) in DCM for 4 h at room temperature. The crude product was then dried at low pressure and purified by silica chromatography and eluted with ethyl acetate/hexane (8:2). Afterward, **12** was treated with 2 mL of HCl/dioxane 4.0 M in 10 mL of ethyl acetate for 2 h at room temperature. The final hydrochloride salt was filtered and dried. A white solid with 99% purity was obtained (yield = 82%). ^{1}H NMR (CD_3OD, 400 MHz): 2.04 (s, 3H), 4.10 (s, 2H), 4.40 (s, 2H), 7.35 (m, 2H), 7.38 (m, 2H). ^{13}C NMR (CD_3OD, 400 MHz): 42.9, 43.0, 127.6, 128.0, 128.17, 129.2, 133.5, 139.7, 172.4. ES+ (m/z): calcd for $C_{10}H_{15}N_2O$ $(M + H)^+$, 126.1179; found, 179.1176.

General Method for the Synthesis of *N*-(3-Aminomethylbenzyl)-acylamide Derivatives. 3-(Boc-aminomethyl)-benzylamine hydrochloride (1 equiv) was dissolved in DMF, and HOBt (1 equiv), the corresponding carboxylic acid (1 equiv), and DIEA (2 equiv) were then added. Next, DIPCDI (1 equiv) was added, and the mixture was stirred for 12 h at room temperature. DMF was then removed at low pressure. The Boc derivative crude product was dissolved in 300 mL of ethyl acetate and washed with 5% $NaHCO_3$ (3 × 100 mL). The organic fractions were washed with brine and dried with $MgSO_4$, and the solvent was removed at low pressure. All the compounds were purified by silica chromatography and eluted with a gradient of ethyl acetate/hexane. Afterward, all the compounds were treated with 2 mL of HCl/dioxane 4.0 M in 10 mL of ethyl acetate for 2 h at room temperature. The final hydrocloride salts were filtered and dried.

***N*-(3-(Aminomethyl)benzyl)propionamide Hydrochloride Salt (31).** A white solid was obtained (yield = 86%) with 100% purity. ^{1}H NMR (CD_3OD, 400 MHz): 1.14 (t, 2H, J = 7.6 Hz), 2.27 (q, 3H, J = 7.6 Hz), 4.10 (s, 2H), 4.38 (s, 2H), 7.352 (m, 2H), 8.43 (s, NH), 7.38 (m, 2H). ^{13}C NMR (CD_3OD, 400 MHz): 9.2, 28.9, 42.5, 43.0, 127.5, 127.9, 128.0, 129.2, 133.4, 140.2, 175.8. ES+ (m/z): calcd for $C_{11}H_{17}N_2O$ $(M + H)^+$, 193.1335; found, 192.1340.

***N*-(3-(Aminomethyl)benzyl)-2-iodoacetamide Hydrochloric Salt (32).** A white solid was obtained (yield = 81%) with 99/97% purity. ^{1}H NMR (CD_3OD, 400 MHz): 4.10 (s, 2H), 4.44 (s, 2H), 7.39 (m, 4H). ^{13}C NMR (CD_3OD, 400 MHz): 41.9, 42.9, 43.0, 127.6, 128.0, 128.1, 129.3, 133.4, 139.6, 168.1. ES+ (m/z): calcd for $C_{10}H_{15}N_2O$ $(M + H)^+$, 126.0714; found, 126.0714.

***N*-(3-(Aminomethyl)benzyl)benzamide Hydrochloride Salt (34).** A white solid was obtained (yield = 85%) with 99% purity.^{1}H NMR (CD_3OD, 400 MHz): 4.10 (s, 2H), 4.60 (s, 2H), 7.36 (m, 1H), 7.42 (m, 2H), 7.43 (m, 3H), 7.54 (m, 1H), 7.85 (m, 2H). ^{13}C NMR (CD_3OD, 400 MHz): 43.0, 43.1, 127.1, 127.5, 128.0, 128.1, 128.4, 129.2, 131.6, 133.4, 134.1, 140.4, 169.0. ES+ (m/z): calcd for $C_{10}H_{15}N_2O$ $(M + H)^+$, 241.1335; found, 241.1335.

***N*-(3-(Aminomethyl)benzyl)-4-hydroxybenzamide Hydrochloride Salt (38).** A white solid was obtained (yield = 84%) with 98% purity. ^{1}H NMR (CD_3OD, 400 MHz): 4.09 (s, 2H), 4.56 (s, 2H), 6.83 (d, 2H, J = 8.7 Hz), 7.33 (m, 1H), 7.41 (m, 2H), 7.43 (s, H), 7.75 (d, 2CH, J = 8.7 Hz). ^{13}C NMR (CD_3OD, 400 MHz): 42.9, 43.1, 114.9, 124.9, 127.4, 127.9, 128.1, 129.1, 129.2, 133.3, 140.6, 161.0, 168.8. ES+ (m/z): calcd for $C_{15}H_{17}N_2O_2$ $(M + H)^+$, 257.1285; found, 257.1280.

***N*-(3-(Aminomethyl)benzyl)-4-bromobenzamide Hydrochloride Salt (39).** A white solid was obtained (yield = 80%) with 100% purity. ^{1}H NMR (CD_3OD, 400 MHz): 4.103 (s, 2H), 4.58 (s, 2H), 7.35 (m, 1H), 7.414 (m, 2H), 7.453 (m, 1H), 7.78 (d, J = 8.68 Hz, 2H), 7.64 (d, J = 8.68 Hz, 2H). ^{13}C NMR (CD_3OD, 400 MHz): 43.1, 43.2, 126.0, 127.5, 128.0, 128.2, 129.0, 129.2, 131.6, 133.2, 133.4, 140.2, 167.8. ES+ (m/z): calcd for $C_{15}H_{16}BrN_2O$ $(M + H)^+$, 319.0441; found, 319.0441.

***N*-(3-(Aminomethyl)benzyl)-4-(aminomethyl)benzamide (40).** A white solid was obtained (yield = 82%) with 100% purity. ^{1}H NMR (CD_3OD, 400 MHz): 4.11 (s, 2H), 4.19 (s, 2H), 4.60 (s, 2H), 7.36 (m, 1H), 7.42 (m, 2H), 7.47 (m, 1H), 7.96 (d, J = 8.39 Hz, 1H), 7.58 (d, J = 8.27 Hz, 1H). ^{13}C NMR (CD_3OD, 400 MHz): 42.6, 43.0, 43.1, 127.6, 128.0, 128.1, 128.9, 129.2, 133.4, 134.8, 136.8, 140.2, 168.0. ES+ (m/z): calcd for $C_{16}H_{21}N_3O$ $(M + H)^+$, 270.1601; found, 270.1596.

***N*-(3-(Aminomethyl)benzyl)Phg(Ac) Hydrochloride Salt (35).** A mixture of of 3-(Boc-aminomethyl)-benzylamine hydrochloride (300 mg, 1 equiv) was dissolved in DMF (100 mL) and HOBt (149 mg, 1 equiv). Fmoc-phenylglycine carboxylic acid (410 mg, 1 equiv) and DIPCDI (162 μL, 1 equiv) were then added. DIEA (204 μL, 1.1 equiv) was then added, and the mixture was stirred for 12 h at room temperature. After that, the DMF was removed at low pressure. The crude of *N*-(3-(aminomethyl)benzyl)Phg(Fmoc) was dissolved in 300 mL of ethyl acetate and washed with 5% $NaHCO_3$

(3 × 100 mL). The organic layers were pooled, washed with brine (3 × 100 mL), and dried with $MgSO_4$, and the solvent was removed at low pressure. *N*-(3-(Aminomethyl)benzyl)Phg(Fmoc) was dissolved in DCM (10 mL). Piperidine 20% in DMF (2 mL) was then added, and the mixture was stirred for 4 h at room temperature. The crude product was then washed with diethyl ether (3 × 100 mL) to remove the dibenzofulvene. *N*-(3-(Aminomethyl)benzyl)-$PhgNH_2$ was dissolved in DCM (100 mL) and acetylated with Ac_2O/DIEA (1:2) for 4 h at room temperature to yield the final product. The crude product was purified by silica chromatography with AcOEt/hexane (8:2, v/v). Afterward, the compound was treated with 2 mL of HCl/dioxane 4.0 M in 10 mL of ethyl acetate for 2 h at room temperature. The final hydrochloride salt was filtered and dried. A white solid was obtained (yield = 70%) with 100% purity. ^{1}H NMR (CD_3OD, 400 MHz): 2.0 (s, 3H), 4.06 (s, 2H), 4.41 (ddd, 2H, J = 5.9 Hz, J = 15.5 Hz, J = 56.6 Hz), 5.36 (s, H), 7.25 (m, 1H), 7.34 (m, 6H), 7.44 (m, 2H), 8.78 (s bb, NH). ^{13}C NMR (CD_3OD, 400 MHz): 19.6, 21.2, 42.4, 43.1, 58.6, 60.3, 127.3, 127.4, 127.7, 127.8, 128.3, 128.6, 129.0, 133.3, 136.9, 139.9, 171.9, 172.1. ES+ (*m*/*z*): calcd for $C_{10}H_{15}N_2O$ $(M + H)^+$, 312.1707; found, 312.1703.

***N*-(3-(Aminomethyl)benzyl)allylcarbamate Hydrocloride Salt (33).** 3-(Boc-Aminomethyl)-benzylamine hydrochloride (300 mg, 1 equiv) was dissolved in DCM. DIEA (932 μL,1 equiv) and allyl chloroformate (88 μL,1 equiv) were then added, and the reaction mixture was stirred for 4 h at room temperature. Afterward, the solvent was evaporated, and the crude product was dissolved in ethyl acetate (300 mL), washed with H_2O (2 × 100 mL) and brine (2 × 100 mL), and dried with $MgSO_4$. The product was dried at low pressure and analyzed by HPLC-MS. The compound was then treated with 2 mL of HCl/dioxane 4.0 M in 10 mL of ethyl acetate for 2 h at room temperature. The final hydrochloride salt was filtered and dried. A white solid was obtained (yield = 92%) with 99% purity. ^{1}H NMR (CD_3OD, 400 MHz): 4.10 (s, 2H), 4.31 (s, 2H), 4.54 (d, 2H, J = 5.4 Hz), 5.24 (dd, 2H, J = 13.9 Hz, J = 47.6 Hz), 5.93 (ddd, 1H, J = 5.4 Hz, J = 10.6 Hz, J = 22.1 Hz), 7.38 (m, 4H), 7.60 (s, NH). ^{13}C NMR (CD_3OD, 400 MHz): 43.1, 43.9, 65.3, 116.3, 127.5, 127.7, 127.8, 129.2, 133.2, 133.4, 140.7, 157.6. ES+ (*m*/*z*): calcd for $C_{12}H_{17}N_2O_2$ $(M + H)^+$, 221.1285; found, 221.1281.

(3-((Tosylamino)methyl)phenyl)methanamonium Hydrochloride Salt (36). An amount of *p*-toluensulfonyl chloride (208 mg, 1.0 equiv) and 3-(Boc-aminomethyl)-benzylamine hydrochloride (300 mg, 1.0 equiv) were dissolved in 20 mL ice-cooled acetone and stirred for 10 min. Afterward, K_2CO_3 (379 mg, 2.5 equiv) dissolved in water (10 mL) was added, and the mixture was stirred for 4 h at room temperature. The solvent was then evaporated, and the crude product was dissolved in ethyl acetate (300 mL). The organic layer was washed with water (3 × 100 mL), and brine (3 × 100 mL), and dried with $MgSO_4$, and the solvent was then removed. The product was dried at low pressure and analyzed by HPLC-MS. Afterward, the Boc derivative was treated with 2 mL of HCl/dioxane 4.0 M in 10 mL of ethyl acetate for 2 h at room temperature. The final hydrochloride salt was filtered and dried. A pale yellow solid was obtained (yield = 86%) with 99% purity. ^{1}H NMR (CD_3OD, 400 MHz): 2.41 (s, 3H), 4.05 (s, 2H), 4.06 (s, 2H), 5.48 (s, SO_2NH), 7.28 (m, 1H), 7.33 (m, 3H), 7.36 (d, 2H, J = 8.4 Hz), 7.73 (d, 2H, J = 8.2 Hz). ^{13}C NMR (CD_3OD, 400 MHz): 20.3, 43.0, 46.3, 126.9, 127.8, 128.2, 128.4, 129.1, 129.5, 133.3, 137.7, 138.9, 143.5. ES+ (*m*/*z*): calcd for $C_{15}H_{19}N_2O_2S$ $(M + H)^+$, 291.1162; found, 291.1161.

Preparation of Mouse Adipose Tissue Membranes. Internal adipose tissue was obtained from Swiss mice weighing between 20 and 25 g. The tissue was cut and homogenized in HES buffer (25 mmol/L HEPES, 2 mmol/l EDTA, 255 mmol/L sucrose) with antiproteases (1 μmol/L pepstatin, 1 μmol/L leupeptin, 0.14 trypsin inhibitor units per mL aproptinin and 1 mmol/L PMSF). Lysates were then centrifuged at 5000 × *g* at 4 °C for 15 min to remove the fat cake and nonhomogenized material, and supernatants were collected and centrifuged at 200 000 × *g* for 2 h at 4 °C. Pelleted membranes were resuspended in 30 mmol/ L HEPES and stored at −80 °C until use. Protein concentrations were measured by the Bradford method with γ-globulin as standard.

Fluorimetric Detection of SSAO-Mediated H_2O_2 Formation. The SSAO activity of human recombinant VAP-1 (0.1 μg protein/assay) and mouse adipose tissue membranes (1 μg protein/assay) was measured using Amplex Red reagent, a highly sensitive and stable probe for H_2O_2.[24] The reaction was performed in 200 μL of 0.2 mol/L phosphate buffer at pH 7.4 for 50 min at 37 °C in black nonphosphorescent microplates (Nunc). Catalytic reaction was initiated by the addition of the amines indicated as putative SSAO substrates and a H_2O_2-detecting mixture containing horseradish peroxidase and Amplex Red, as previously described.[15] Fluorescence intensity was measured (excitation, 545 nm; emission, 590 nm; Bio-Tek fluorescence plate reader), and H_2O_2 concentration was calculated from calibration curves generated by serial dilutions of standard H_2O_2. Fluorescence readings were performed every 5 min. SSAO-independent H_2O_2 production was measured by preincubating adipocyte membranes or human SSAO protein with 250 μM semicarbazide for 20 min to totally inhibit SSAO activity, and fluorescence values were subtracted from the total amount of H_2O_2 formed. The kinetic parameters (K_m and V_{max}) were calculated using appropriate nonlinear curve-fitting formula following the Michaelis−Menten equation and using GraphPad Prism 4.0 software.

Glucose Transport Measurements in Isolated Mouse Adipocytes. Adipocytes were isolated from internal fat pads of healthy male Swiss mice (30−35 g) by digestion in KRBHA containing 0.66 mg colagenase/mL.[4,5] After a preincubation period of 45 min at 37 °C, each vial, which contained 200 μL of cell suspension in KRBHA and the drugs being tested, received an isotopic dilution of 2-deoxy-D-[^{3}H]glucose (2-DG), giving a final concentration of 0.1 mM, equivalent to approximately 1 300 000 dpm/vial. 2-DG transport assays were performed as reported.[4,5] The values of basal transport represented 0.33 ± 0.03 nmol 2-DG/mg lipid/10 min.

Molecular Modeling and Docking. Homology modeling of the biological dimer of mouse SSAO was performed on the basis of the crystallographic structure of homologous human SSAO (83.8% sequence identity), whose coordinates are deposited in the Protein Data Bank (PDB) with code 1us1.[25−27] Given the high sequence identity between mouse and human SSAO, no other template was used. We followed the standard protocol in Modeler.[15] Fifteen side chains were automatically placed by the default procedure, followed by a standard minimization in Modeler, with no additional restraints applied to the active site or to any other part of the structure. The five lowest-scoring conformations were automatically selected according to the Modeler objective function. From these five conformations, as our final model, we selected the one that yielded the best values of PROCHECK test.[28] This model was subjected to molecular dynamics simulations using NAMD with ff99 parameterization.[29,30] Molecular dynamics of the mouse SSAO model built was performed with a protocol comprising an initial 10 000-step conjugate gradient minimization in full explicit solvent, followed by 100 ps of equilibration (gradually reducing positional restraints on protein atoms, with no restraints on explicit solvent atoms) and finally 200 ps of free molecular dynamics in full explicit solvent at constant temperature (T = 300 K). Protein was placed in a truncated octahedron box filled by water molecules, and all atoms (protein and solvent) were free to move during the molecular dynamics step. The complete protocol took around 50 h in 16 CPUs (Intel Xeon 2.80 MHz). The model was stable throughout both the equilibration and the molecular dynamics phases, in which atomic coordinates remained mostly within 1.6 Å of RMSD from the initial coordinates. The same protocol was applied to the X-ray structure of human SSAO, yielding similarly stable dynamics. Selected molecules for docking (**1**, **34**, **41**, **42**, **44**) were minimized in the MM3 force field using TINKER.[31,32] Conformational sampling of these molecules was performed by molecular dynamics in the MM3 force field, as implemented in TINKER, a molecular modeling package previously developed in our laboratory.[33] For each of these conformations, CMIP performed an exhaustive rotational and

translational search in a series of steps for which the binding energy is computed using binding potentials precalculated on a 3D grid (0.5 Å grid step) within a box of size of $30 \times 28 \times 24$ Å^3 covering the full SSAO active site. These binding energy potentials accounted for the Lennard−Jones van der Waals interactions and the Poisson−Boltzmann electrostatics, with ff99 parameterization.[20] In addition to the one in the X-ray structure (PDB code 1us1), several conformational states of SSAO were considered, for which a number of models were generated as follows. Two conformations of the TPQ residue were considered: on-copper inactive conformation (the one in the X-ray structure of human SSAO) and off-copper active conformation (with coordinates taken from bovine SSAO with modified residue mimicking benzylamine covalently attached to the TPQ). To roughly mimic the flexibility of the binding pocket, an alternative side-chain rotamer was considered for the Leu469 residue, in addition to that in the X-ray structure. The TPQ residue was parameterized using LEAP from Amber, with atomic charges calculated by Gaussian 03 (www.Gaussian.com).[34] Binding energy potentials were calculated by CMIP on a 3D grid around the SSAO active site residues. Given that the protein coordinates were fixed during each docking simulation, the van der Waals radii of protein and substrate atoms were scaled by a factor of 0.8, to avoid strong clashes derived from the suboptimal geometries of the docked orientations.

Acknowledgment. This study was supported by research grants from the Ministerio de Ciencia y Tecnología (SAF2002-02125, SGR01-118, BQU2002-02047, CTQ2005-0315, and BQU2003-00089), Grant SGR01-118 from the Generalitat de Catalunya, the Fundació Marató de TV3 (300720), and from the Instituto de Salud Carlos III RCMN (C03/08), RGDM (G03/212), and RGTO (G03/028), the Generalitat de Catalunya (Grup Consolidat and Centre de Referència en Biotecnologia), and the Barcelona Science Park. J.F.-R. is supported by the Ramon y Cajal program (Ministerio de Ciencia y Tecnología, Spain). We thank Molsoft for the use of ICM-Browser and Modesto Orozco and Josep Lluis Gelpi for useful comments and the use of CMIP. NAMD was developed by the Theoretical and Computational Biophysics Group in the Beckman Institute for Advanced Science and Technology at the University of Illinois at Urbana-Champaign. We thank Tanya Yates for her editorial support.

Supporting Information Available: Combinatorial chemistry, preliminary biological HPLC data, purity data table, and spectroscopy data (^{1}H/^{13}C NMR) of selected compounds. This material is available free of charge via the Internet at http://pubs.acs.org

References

(1) Murray, M. J.; Saysell, C. G.; Wilmot, C. M.; Tambyrajah, W. S.; Jaeger, J.; Knowles, P. F.; Pillips, S.; McPherson, M. J. The active site base controls cofactor reactivity in *Escherichia coli* amine oxidase: X-ray crystallographic studies with mutational variants. *Biochemistry* **1999**, *38*, 8217−8227.

(2) Jalkannen, S.; Salmi, M. Cell surface monoamine oxidases: enzymes in search of a function. *EMBO J.* **2001**, *20*, 3893−3901.

(3) Morris, N. J.; Ducret, A.; Aebersold, R.; Ross, S. A.; Keller, S. R.; Lienhard, G. E. Membrane amine oxidase cloning and identification as a major protein in the adipocyte plasma membrane. *J. Biol. Chem.* **1997**, *272*, 9388−9392.

(4) Enrique-Tarancón, G.; Marti, L.; Morin, M.; Lizcano, J., M.; Unzeta, M.; Sevilla, L.; Camps, M.; Palacín, M.; Testar, X.; Carpéné, C.; Zorzano, A. Role of semicarbazide-sensitive amine oxidase on glucose transport and GLUT4 recruitment to the cell surface in adipose cells. *J. Biol. Chem.* **1998**, *273*, 8025−8032.

(5) Marti, L.; Morin, M.; Enrique-Tarancón, G.; Prevot, D.; Lafontan, M.; Testar, X.; Zorzano, A.; Carpéné, C. Tyramine and vanadate synergistically stimulate glucose transport in rat adipocytes by amine oxidase-dependent generation of hydrogen peroxide. *J. Pharmacol. Exp. Ther*. **1998**, *285*, 342−349.

(6) Morin, M.; Visentin, V.; Calisse, D.; Marti, L.; Zorzano, A.; Testar, X.; Valet, P.; Fischer, Y.; Carpéné, C. Tyramine stimulates glucose uptake in insulin-sensitive tissues in vitro and in vivo via its oxidation by amine oxidases. *J. Pharmacol. Exp. Ther*. **2002,** *303*, 1238−1247.

(7) Morin, N.; Lizcano, J. M.; Fontana, E.; Marti, L., Smih, F.; Rouet, P.; Prevot, D.; Zorzano, A.; Unzeta, M.; Carpéné, C. Semicarbazide-sensitive amine oxidase substrates stimulate glucose transport and inhibit lipolysis in human adipocytes. *J Pharmacol. Exp. Ther*. **2001**, *297*, 563−572.

(8) Fontana, E.; Boucher, J.; Marti, L.; Lizcano, J. M.; Testar, X., Zorzano, A.; Carpéné, C. Amine oxidase substrates mimic several of the insulin effects on adipocyte differentiation in 3T3 F442A cells. *Biochem J.* **2001**, *356*, 769−777.

(9) Abella, A.; Marti, L.; Camps, M.; Claret, M.; Fernández-Alvarez, J.; Gomis, R.; Gumà, A.; Viguerie, N.; Carpéné, C.; Palacín, M.; Testar, X.; Zorzano, A. Semicarbazide-sensitive amine oxidase/vascular adhesion protein-1 activity exerts an antidiabetic action in Goto−Kakizaki rats. *Diabetes* **2003**, 52, 1004−1013.

(10) Marti, L.; Abella, A.; Carpéné, C.; Palacín, M.; Testar, X.; Zorzano, A. Combined treatment with benzylamine and low dosages of vanadate enhances glucose tolerance and reduces hyperglycemia in streptozotocin-induced diabetic rats. *Diabetes* **2003**, *50*, 2061−2068.

(11) Zorzano, A.; Abella, A.; Marti, L.; Carpéné, C.; Palacín, M.; Testar, X. Semicarbazide-sensitive amine oxidase activity exerts insulin-like effects on glucose metabolism and insulin-signaling pathways in adipose cells. *Biochim. Biophys. Acta* **2003**, *1647*, 3−9.

(12) Yu, P. H.; Zuo, D. M. Oxidative deamination of methylamine by semicarbazide-sensitive amine oxidase leads to cytotoxic damage in endothelial cells. Possible consequences for diabetes. *Diabetes* **1993**, *42*, 594−603.

(13) Marti, L.; Abella, A.; De la Cruz, X.; García-Vicente, S.; Unzeta, M.; Carpéné, C.; Palacín, M.; Testar, X.; Orozco, M.; Zorzano, A. Exploring the binding mode of semicarbazide-sensitive amine oxidase/VAP-1: identification of novel substrates with insulin-like activity. *J. Med. Chem*. **2004**, *47*, 4865−4874.

(14) Bair, K. W.; Tuttle, R. L.; Knick, V. C.; Cory, M.; McKee, D.D. [(1-Pyrenylmethyl)amino]alcohols, a new class of antitumor DNA intercalators. Discovery and initial amine side chain structure−activity studies. *J. Med. Chem*. **1990**, *33*, 2385−2393.

(15) Scozzafava, A.; Supuran, C. T. Carbonic anhydrase and matrix metalloproteinase inhibitors: sulfonylated amino acid hydroxamates with MMP inhibitory properties act as efficient inhibitors of CA isozymes I, II, and IV, and *N*-hydroxysulfonamides inhibit both these zinc enzymes. *J. Med. Chem.*, **2000**, *43*, 3677−3687.

(16) Lyles, G. A. Substrate-specificity of mammalian tissue-bound semicarbazide-sensitive amine oxidase. *Prog. Brain Res.* **1995**, *106*, 293−303.

(17) Wilce, M. C. J.; Dooley, D. M.; Freeman, H. C.; Guss, J. M.; Matsunami, H.; McIntire, W. S.; Ruggiero, C. E.; Tanizawa, K.; Yamaguchi, H. Crystal structures of the copper-containing amine oxidase from Arthrobacter globiformis in the holo and apo forms: implications for the biogenesis of topaquinone. *Biochemistry* **1997**, *36*, 16116−16133.

(18) Salminen, T. A.; Smith, D. J.; Jalkanen, S.; Johnson, M. S. Structural model of the catalytic domain of an enzyme with cell adhesion activity: human vascular adhesion protein-1 (HVAP-1) D4 domain is an amine oxidase. *Protein Eng*. **1998**, *11*, 1195−1204.

(19) Lunelli, M.; Di Paolo, M. L.; Biadene, M.; Calderone, V.; Battistutta, R.; Scarpa, M.; Rigo, A.; Zanotti, G. Crystal structure of amine oxidase from bovine serum. *J. Mol. Biol.* **2005**, *346*, 991−1004.

(20) Liang, J.; Edelsbrunner, H.; Woodward, C. Anatomy of protein pockets and cavities: measurement of binding site geometry and implications for ligand design. *Protein Sci.* **1998**, *7*, 1884−1897.

(21) Salmi, M.; Yegutkin, G. G.; Lehvonen, R.; Koskinen, K.; Salminen, T.; Jalkanen, S. A cell surface amine oxidase directly controls lymphocyte migration. *Immunity* **2001**, *14*, 265−276.

(22) Lyles, G. A. Substrate-specificity of mammalian tissue-bound semicarbazide-sensitive amine oxidase. *Prog. Brain Res*. **1995**, *106*, 293−303.

(23) Wilmot, C. M.; Murray, J. M.; Alton, G.; Parsons, M. R.; Convery, M. A.; Blakeley, V.; Corner, A. S.; Palcic, M. M.; Knowles, P. F.; McPherson, M. J.; Phillips, S. E. V. Catalytic mechanism of the quinoenzyme amine oxidase from *Escherichia coli*: exploring the reductive half-reaction. *Biochemistry* **1997**, *36*, 1608−1620.

(24) Zhou, M.; Panchuk-Voloshina, N. A one-step fluorometric method for the continuous measurement of monoamine oxidase activity. *Anal. Biochem.* **1997**, *253*, 169−174.

(25) Sali, A.; Blundell, T. L. Comparative protein modeling by satisfaction of spatial restraints. *J. Mol. Biol*. **1993**, *234*, 779−815.

(26) Bernstein, F. C.; Koetzle, T. F.; Williams, G. J.; Meyer, E. F., Jr.; Brice, M. D.; Rodgers, J. R.; Kennard, O.; Shimanouchi, T.; Tasumi, M. The protein data bank: a computer-based archival file for macromolecular structures. *J. Mol. Biol*. **1977**, *112*, 535−542.
(27) Airenne, T. T.; Nymalm, Y.; Kidron, H.; Smith, D. J.; Pihlavisto, M.; Salmi, M.; Jalkanen, S.a; Johnson, M. S.; Salminen, T. A. Crystal structure of the human vascular adhesion protein-1: Unique structural features with functional implications. *Protein Sci.* **2005**, *14*, 1964−1974.
(28) Laskowski, R. A.; MacArthur, M. W.; Moss, D. S.; Thornton, J. M. PROCHECK: a program to check the stereochemical quality of protein structures. *J. Appl. Crystallogr.* **1993**, *26*, 283.
(29) Phillips, J. C.; Braun, R.; Wang, W.; Gumbart, J.; Tajkhorshid, E.; Villa, E.; Chipot, C.; Skeel, R. D.; Kale, L.; Schulten, K. Scalable molecular dynamics with NAMD. *J. Comput. Chem.* **2005**, *26*, 1781−1802.
(30) Wang, J.; Cieplak, P.; Kollman, P. A. How well does a restrained electrostatic potential (RESP) model perform in calculating conformational energies of organic and biological molecules? *J. Comput. Chem.* **2000**, *21*, 1049−1074.
(31) Allinger, N. L.; Yuh, Y. H.; Lii, J. H. Molecular mechanics. The MM3 force field for hydrocarbons. 1. *J. Am. Chem. S*oc. **1989**, *111*, 8551−8566.
(32) Ponder, J. W.; Richards, F. M. An efficient Newton-like method for molecular mechanics energy minimization of large molecules. *J. Comput. Chem.* **1987**, *8*, 1016−1024.
(33) Gelpi, J. L.; Kalko, S. G.; Barril, X.; Cirera, J.; de La Cruz, X.; Luque, F. J.; Orozco, M. Classical molecular interaction potentials: improved setup procedure in molecular dynamics simulations of proteins. *Proteins* **2001**, *45*, 428−437.
(34) Pearlman, D. A.; Case, D. A.; Caldwell, J. W.; Ross, W. S.; Cheatham, T. E., III; DeBolt, S.; Ferguson, D.; Seibel, G.e; Kollman, P. "AMBER", a package of computer programs for applying molecular mechanics, normal-mode analysis, molecular dynamics and free energy calculations to stimulate the structural and energetic properties of molecules. *Comput. Phys. Commun*. **1995**, *91*, 1−42.

JM051076E